Supplementary Information for:

Investigating the Mechanism of Post-Treatment on PEDOT:PSS via Single-Particle Absorption Spectroscopy

*Morgan T. Rea, Feng Pan, Erik H. Horak, Kassandra A. Knapper, Hoang L. Nguyen, Cecilia H. Vollbrecht, Randall H. Goldsmith**

Department of Chemistry, University of Wisconsin-Madison, Madison, WI 53706, USA
*Email: Randall Goldsmith, rhg@chem.wisc.edu

Sample Preparation and Treatment Conditions: For the total collected data set of PEDOT:PSS particles shown in the main text, a total of 36 toroidal microresonators over 4 chips (labelled 4I, 2O, 3H, 4J) were used to collect 147 PEDOT:PSS particles in the pristine data set. For thermal treatment conditions, see Methods. For DMSO treatment, 80-100 μL of HPLC or biology grade DMSO was pipetted on the toroid chip, wetting the whole chip, and was left to stand for 5 minutes, then spun at 4000 rpm for 60-120 seconds to dry the chips. Sometimes, an additional spin-coating at 5300 rpm was needed to completely dry the DMSO off the chip. Sometimes, DMSO introduced additional large contaminants, and any objects overwhelmed by the photothermal signal of contaminants were excluded from the DMSO data set. Differences between data sets from different chips for the M and σ values as well as their changes are plotted below and show no significant differences (Figure S1). Spin-coating was used rather than air drying or heating because of concerns of the longer DMSO exposure's ability to completely solubilize and wash away all the particles on the resonator.

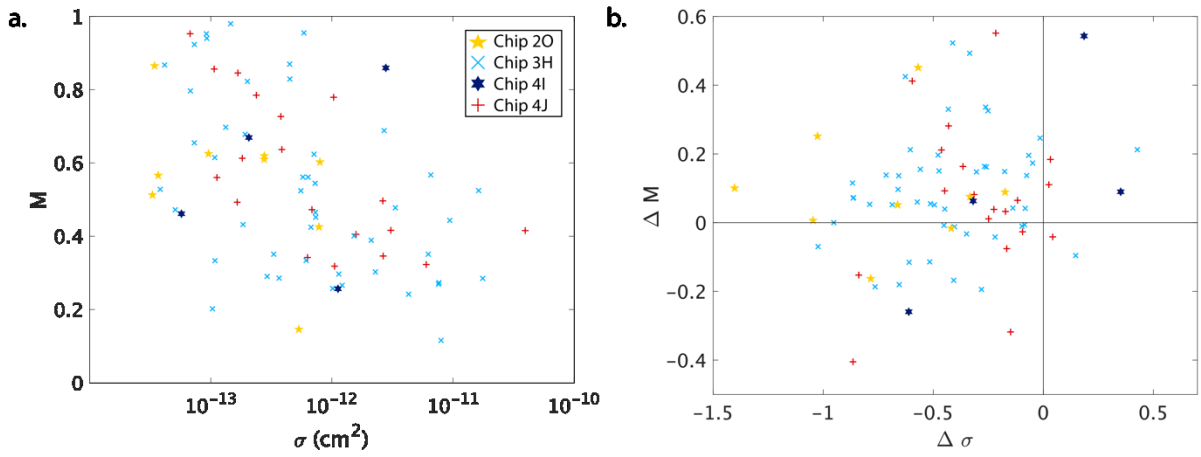

Figure S1. a) Experimentally observed values of M vs. σ and b) ΔM vs. Δσ for Chip 2O (-), Chip 3H (-), Chip 4I (-), and Chip 4J (-).

Calculations: As stated in the main text, the average absorption cross section (σ) for a given particle was calculated by averaging the absorption cross section spectrum over the wavelength range from 1285 nm to 1335 nm, truncating the ends of the laser's tunability range due to noise from low laser power at the ends of its spectral range. Because the cross sections of the particles measured span several orders of magnitude, the absorption cross sections are plotted on a log scale. The changes in absorption cross section after a given treatment is also given as a log plot: $\Delta\sigma=\log_{10}(\sigma_{\text{after treatment}}/\sigma_{\text{before treatment}})$, where $\sigma_{\text{before treatment}}$ is the absorption cross section of the particle before a given treatment, and $\sigma_{\text{after treatment}}$ is the absorption cross section of the particle after a treatment. Thus, $\Delta\sigma_{\text{post-heat}}=\log_{10}(\sigma_{\text{post-heat}}/\sigma_{\text{pristine}})$ and $\Delta\sigma_{\text{post-DMSO}}=\log_{10}(\sigma_{\text{post-DMSO}}/\sigma_{\text{post-heat}})$.

The depth of modulation (M) was found as previously described[1-2] similar to studies of fluorescent polymers[1, 3]. The polarization dependent absorbance was fit to the following equation: $\sigma(\theta)=\sigma_{max}(1 - M \sin^2(\theta - \theta_{max}))$, where $\sigma(\theta)$ is the absorption cross section at a given polarization angle of the pump beam's linearly polarized light. σ_{max} is the maximum absorption cross section at the pump polarization angle θ_{max}, referred to as a particle's peak angle. M is the

depth of modulation with M=1 indicating well aligned chromophores and M=0 indicating poorly aligned chromophores.

The difference in depth of modulation is given by: $\Delta M = M_{\text{after treatment}} - M_{\text{before treatment}}$, where $M_{\text{before treatment}}$ is a particle's depth of modulation before treatment, and $M_{\text{after treatment}}$ is the depth of modulation after a given treatment. Thus, $\Delta M_{\text{post-heat}} = M_{\text{post-heat}} - M_{\text{pristine}}$ and $\Delta M_{\text{post-DMSO}} = M_{\text{post-DMSO}} - M_{\text{post-heat}}$.

Between treatments, the pump polarization angle at which maximum absorption occurred, referred to as peak angle or θ_{max}, would change. As rotating pump polarization is equivalent for two angles 180° apart (e.g. a pump beam polarization of 30° and 210° will yield equivalent absorbance signals of a given particle within error), the two θ_{max} that were found while rotating the half wave plate 360° were considered equivalent. This change in peak angle was calculated using: $\Delta\theta_{max}=|(\theta_{\text{max after treatment}} - \theta_{\text{max before treatment}} + 90) \bmod 180)|$, where mod is a modulus that takes the remainder after dividing $(\theta_{\text{max after treatment}} - \theta_{\text{max before treatment}} + 90)$ by 180. $\theta_{\text{max before treatment}}$ is the pump polarization angle at which maximum absorption occurs before a given treatment, and $\theta_{\text{max after treatment}}$ is the peak angle after treatment, so that: $\Delta\theta_{\text{max post-heat}}=|(\theta_{\text{max post-heat}} - \theta_{\text{max pristine}} + 90) \bmod 180)|$, and $\Delta\theta_{\text{max post-DMSO}}=|(\theta_{\text{max post-DMSO}} - \theta_{\text{max post-heat}} + 90) \bmod 180)|$.

Simulations: The ΔM and $\Delta\sigma$ for a particle of initial M and σ were simulated using a previously developed simulation that modelled the average order for PEDOT:PSS oligomers[2]. This simulation is similar to models that track rotational motion of colloidal clusters[4]. As stated in the main text, a PEDOT:PSS particle is modeled by first randomly assigning an initial orientation of a dipole (representing a chromophore) in spherical coordinates. These spherical coordinates include a θ chosen from a square distribution between 0° and 360° and a φ taken from a square

distribution of cos(φ) from -1 to 1. Once an initial orientation of the chromophore (represented as a unit vector) has been chosen, another chromophore is added to the end of the previous chromophore. The orientation of this previous chromophore is determined by randomly rotating the previous chromophore about the Cartesian coordinate system x (R_x), y (R_y), and z (R_z) represented by:

$$\begin{bmatrix} x_{i+1} \\ y_{i+1} \\ z_{i+1} \end{bmatrix} = R_x(\Delta)R_y(\Delta)R_z(\Delta)\begin{bmatrix} x_i \\ y_i \\ z_i \end{bmatrix}$$

where the coordinate system is represented as:

$$R_x(\Delta) = \begin{bmatrix} 1 & 0 & 0 \\ 0 & \cos(\Delta) & -\sin(\Delta) \\ 0 & \sin(\Delta) & \cos(\Delta) \end{bmatrix};\ R_y(\Delta) = \begin{bmatrix} \cos(\Delta) & 0 & \sin(\Delta) \\ 0 & 1 & 0 \\ -\sin(\Delta) & 0 & \cos(\Delta) \end{bmatrix};$$

$$R_z(\Delta) = \begin{bmatrix} \cos(\Delta) & -\sin(\Delta) & 0 \\ \sin(\Delta) & \cos(\Delta) & 0 \\ 0 & 0 & 1 \end{bmatrix}$$

The angular deviation (Δ) for a given chromophore from its previous chromophore is determined from a Gaussian weighted number generator centered at zero with a standard deviation of Δ=2.4º. This standard deviation Δ=2.4º was calculated by fitting the DMSO treated M and σ values for all of the particles to a logistic function: $M = \frac{1}{(1+10^{(\sigma-\beta)})}$, where M is the depth of modulation; σ is the absorption cross section; and β is the 50% falloff of the logistic function representing average relative chromophore alignment for PEDOT:PSS. This β value can be compared previous simulations[2] which determined β values based on a given angular deviation with standard deviation of Δ. The logistic function fit to the data yielded β=-12.2 which matched with an angular deviation of 2.4º. This β value matches previously obtained values in past studies where β=-12.17.[2] Adding these chromophores sequentially from the previous chromophore with a deviation determined from a Gaussian probability creates a random walk of

absorbing chromophores. From this model, the angular dependence of the 2D intensity in the xy plane is calculated, reflecting experimental conditions where the linearly polarized pump beam is rotated to maximize absorption and generate the angular dependence needed to calculate M. From this angular dependence of the 2D intensity, M and the maximum intensity at θ_{max} are calculated. Each unit in the random walk represents one bipolaron chromophore, so the 2D intensity is later converted to σ by multiplying each chromophore by 4.2×10^{-16} cm^2 which is the absorption cross section of a single bipolaron chromophore.[2, 5] The 2D intensity is calculated by:

$$I_i(\theta)=\sin^2(\phi_i)\cos^2(\theta-\theta_i)$$

where $I_i(\theta)$ is the 2D intensity of a given chromophore i, and θ_i and ϕ_i are spherical coordinates of a given chromophore. The angular rotation of the pump beam is represented by θ and is sampled from 0 to 180^o to generate the angular dependence of intensity. The total 2D intensity of a given chain is represented as the sum of individual chromophore 2D intensities. Because chains were incrementally increased in size by orders of magnitudes, gaps between the initial chains sizes are observed since only discrete values of chromophore lengths were sampled.

After the initial M and σ were calculated, approximately 61% of chromophores were deleted in various ways. With the remaining chromophores, M and σ were recalculated and the ΔM and $\Delta\sigma$ were calculated from the M and σ values before and after chromophore deletion (Figure S2). The chromophores were deleted using various methods described in the main text. In addition to the methods described in the main text, consecutive chromophores were also deleted in set size portions of 10 continuous portions of chromophores. In other words, one random oscillator was selected and then the 10 consecutive oscillators chosen around that randomly selected chromophores were deleted. This was repeated again until at least 61% of the chromophores were deleted, referred to as deletion of portions by set size. Duplicates of deleted

chromophores were removed so that an already selected and deleted chromophore was not doubly counted if selected and deleted again. Because continuous portions of chromophores were deleted from one randomly chosen and over half of the chromophores were deleted, it was possible that consecutive portions greater than 10 oscillators in length were deleted. Despite these slight differences in deletion, the average $\Delta\sigma$ remained close to the experimentally observed value (Table 1 below). Also, because consecutive portions were deleted until at least 61% of chromophores were deleted, sometimes slightly over 61% of chromophores were deleted. A simulation was run where portions of 100 consecutive chromophores in size were deleted. Finally, all chromophores were deleted except for consecutive portions of 39% of chromophores at the end of the length of the chromophore chain representative of PEDOT:PSS. The results of these simulations are shown below.

Table S1. Comparison of $\Delta\sigma$ and ΔM values for different types of simulated chromophore deletions and experimentally observed values

Conditions of Deletion	$\Delta\sigma$	ΔM
Experimentally observed values for after DMSO treatment	-0.408	0.088
Random Deletion of single chromophores	-0.408	0.001
Deletion of 10 consecutive chromophores portions	-0.410	0.004
Deletion of 100 consecutive chromophores portions	-0.438	0.027
Deletion of 100 consecutive chromophores portions excluding particles with only 100 initial chromophores	-0.403	0.027
Deletion of consecutive chromophores in 2% portions of the total number of chromophores	-0.404	0.027
Deletion of consecutive chromophores in 10% portions of the total number of chromophores	-0.410	0.052
Deletion of consecutive chromophores in 20% portions of the total number of chromophores	-0.434	0.058
Deletion of consecutive chromophores in 33.3% portions of the total number of chromophores	-0.425	0.065
Deletion of 61% of chromophores at the end of the simulated polymer chain (first 39% of chromophores kept)	-0.377	0.084
Deletion of 61% of chromophores at the beginning of the simulated polymer chain	-0.374	0.081
Changing angular deviation from $\Delta=2.4^{o}$ to $\Delta=2.0^{o}$ with no deletion of chromophores	0.0560	0.0235

Deletion of 61% of chromophores at the end of the simulated polymer chain and changing angular deviation from $\Delta=2.4^{o}$ to $\Delta=2.0^{o}$ with remaining chromophores.	-0.3221	0.1078

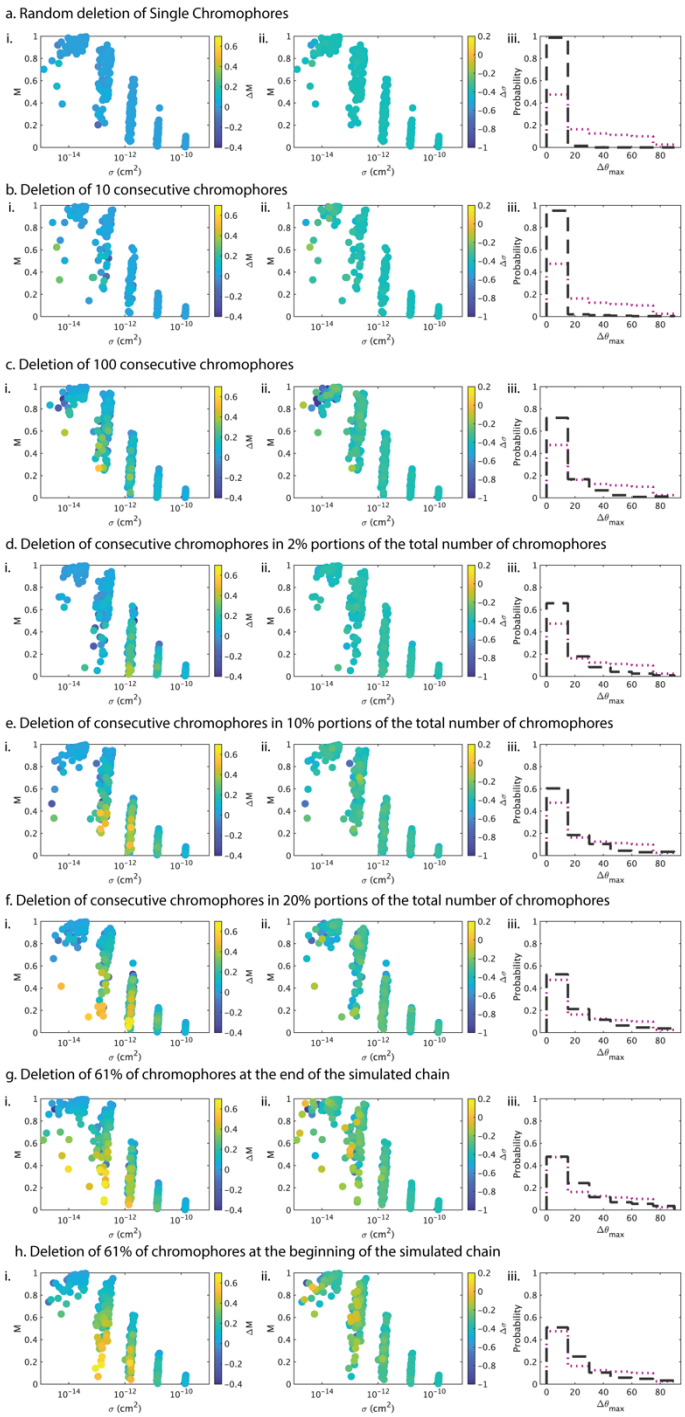

Figure S2. Color plots of the i) ΔM and ii) Δσ after varied chromophore deletions for each particle plotted against the simulated M and σ of each particle before chromophore deletion. iii) Histograms of simulated $\Delta\theta_{max}$ (■) are compared to the experimentally observed values (■). Different methods of deleting chromophores are simulated including: a) Randomly deleting single chromophores. b) Deleting 10 consecutive chromophores in one portion. c) Deleting 100 consecutive chromophores in one portion. d) Deleting consecutive chromophores that are 2% the size of the total number of chromophores. e) Deleting consecutive chromophores that are 10% the size of the total number of chromophores. f) Deleting consecutive chromophores that are 20% the size of the total number of chromophores. g) Deleting 61% of chromophores at the end of the chain. h) Deleting 61% of chromophores at the beginning of the chain.

Variability in Simulations: Additional simulations which model the rotational order of PEDOT:PSS were also run varying the standard deviation of the angular deviation (Δ) and the number of chromophores deleted. These additional simulations were run to see how sensitive the trend (where smaller objects with low structural order increase M) was to the average deviation between consecutive chromophores or the fraction of chromophores deleted. To see if this trend could be reproduced while varying the angular deviation (Δ), simulations as described above

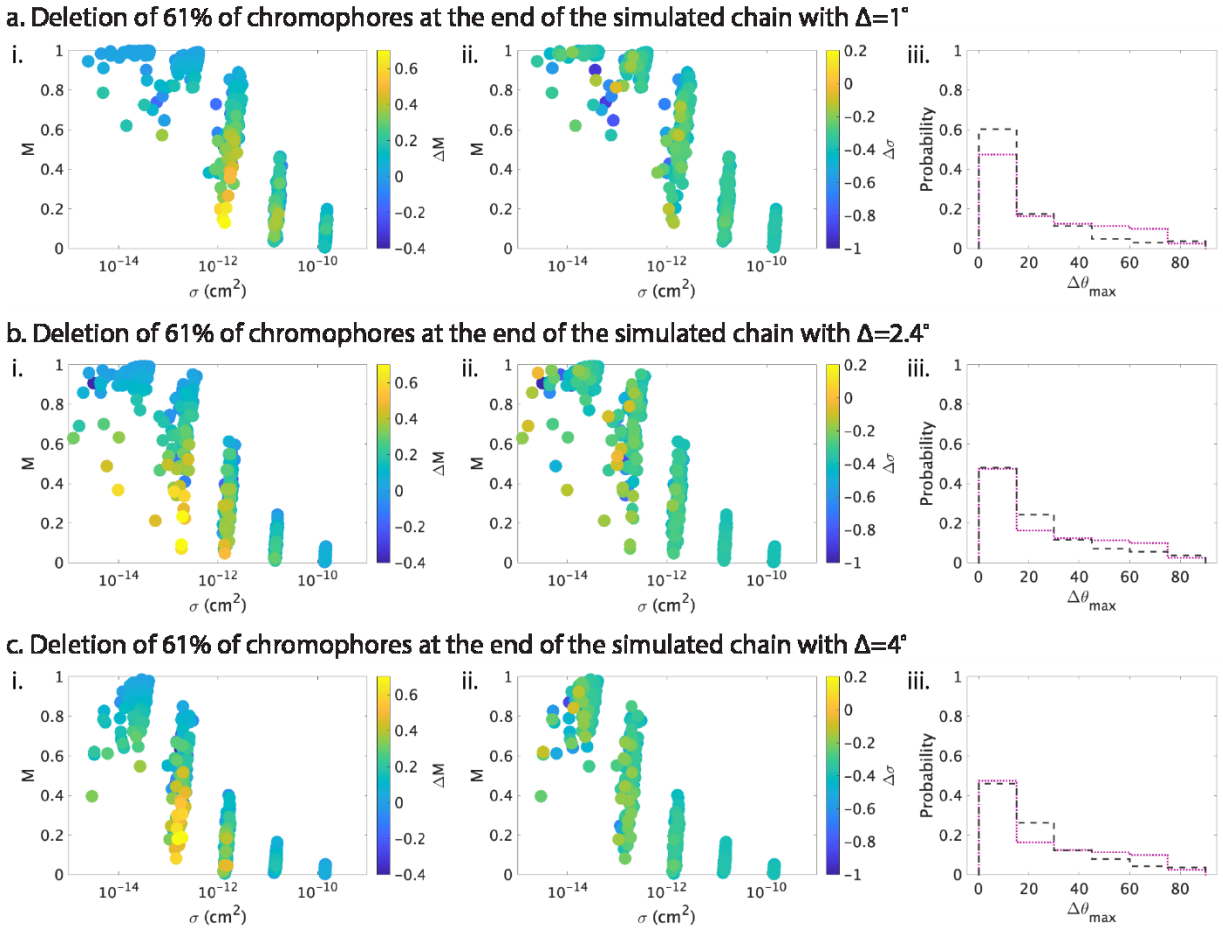

Figure S3. Color plots of the i) ΔM and ii) Δσ after chromophore deletions for each particle plotted against the simulated M and σ of each particle before chromophore deletion. Histograms (iii) of simulated peak angle changes (■) are compared to the experimentally observed values (■). Chromophores were deleted in one continuous portion at the end of the simulated chain. The size of this deleted portion was 61% of the total number of chromophores for a given chain of chromophores. The angle deviations were varied so that a) Δ=1°, b) Δ=2.4° (in main text), and b) Δ=4°.

were run using angular deviations from a Gaussian distribution with a standard deviation of $\Delta=1^{o}$, $\Delta=2.4^{o}$ (in main text), $\Delta=4^{o}$ (Figure S3). Because the trend of increased M after deletion was seen most clearly by deleting continuous portions, simulations were run deleting all chromophores but a continuous portion of the first 39% of chromophores at the beginning of the simulated chain. Although there are differences in the distributions of $\Delta\theta_{max}$, the trend was roughly preserved for all simulations that vary in angular deviation, showing that our conclusions are robust to the average angular deviation used in the simulation. Additional simulations were also run varying the amount of the chromophores deleted to see if the trend was preserved (Figure S4). With $\Delta=2.4^{o}$ kept constant, deleted portions that were 75%, 61%, and 50% of the total number of chromophores were deleted from the end of the simulated polymer chain. The trend where smaller, disordered particles tend to increase M is also roughly preserved showing that variations in the amount deleted also do not drastically change conclusions.

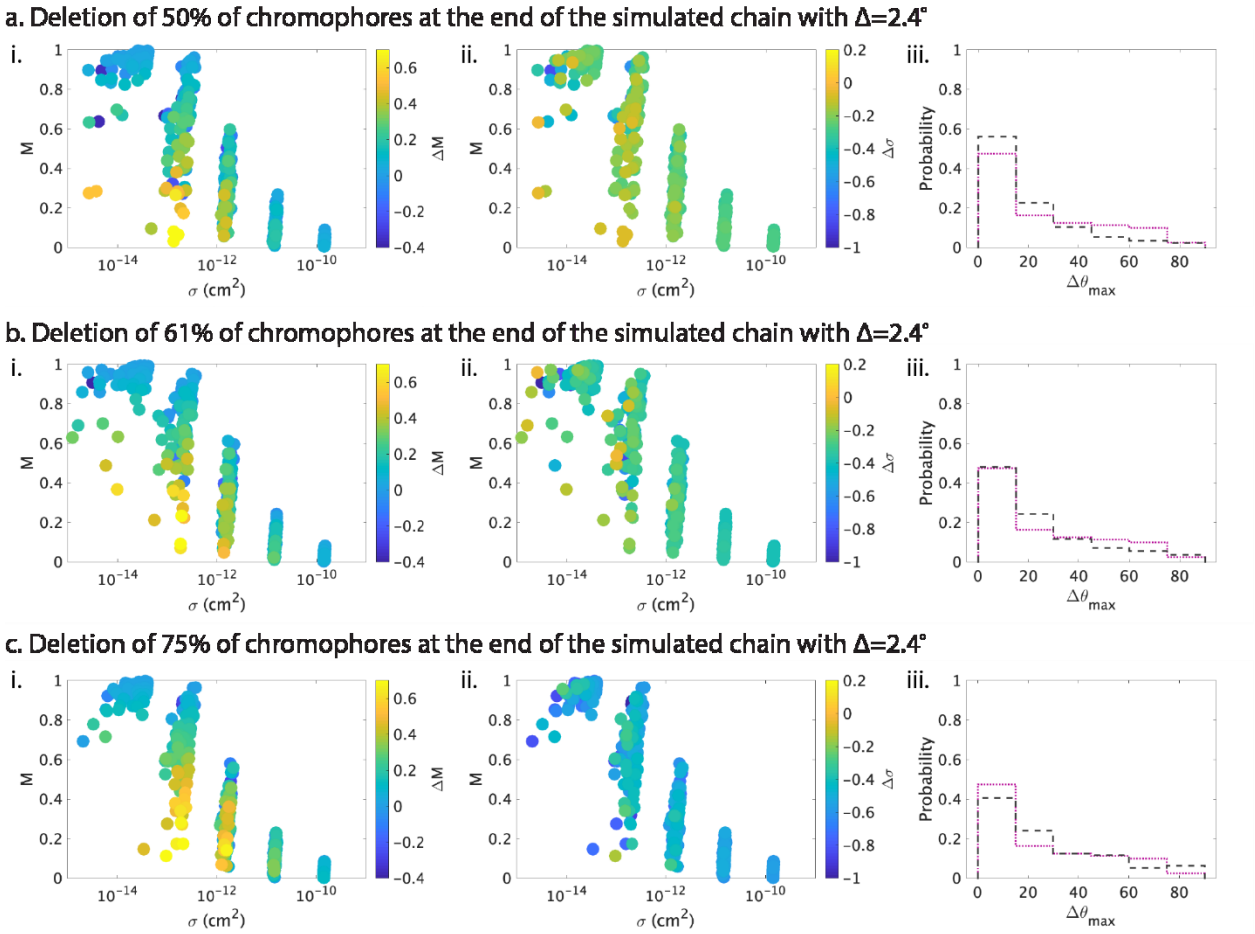

Figure S4. Color plots of the i) ΔM and ii) Δσ after varied chromophore deletions for each particle plotted against the simulated M and σ of each particle before chromophore deletion. Histograms (iii) of simulated peak angle changes (■) are compared to the experimentally observed values (■). Chromophores were deleted in one continuous portion at the end of the simulated chain. The size of deleted portions were a) 50%, b) 61%, and c) 75% of the total number of chromophores.

Chromophore rotation: To see whether or not rotation of chromophores alone could explain the experimental trends, simulations were performed where chromophores were rotated by performing another random walk with more constricted angular deviation instead of deleting chromophores (Figure S5). To do this, a random walk of chromophores was "built" as described above and in the main text and represented the initial polymer chain. A Δ=2.4° was used for the initial random walk of polymers. Then, another random walk of the same length of chromophores was created but with a decreased Δ value of Δ=2.0° to represent a rotation of all

oligomers that leads to an increased alignment of chromophores. Although the trend where smaller, poorly ordered polymers tend to increase M was preserved, the average absorption cross section actually increases, in contrast to experimentally observed values (Table S1). Furthermore, the distribution of $\Delta\theta_{max}$ values also differs from the experimentally observed distributions if only chromophore rotation occurs. This collection of differences suggests that rotation of chromophores leading to increased rotational alignment cannot fully explain the experimentally observed trends alone. Deletion of chromophores was included in another simulation so that the last 61% of chromophores on a chain are deleted and then the remaining chromophores are rotated changing the angular deviation from $\Delta=2.4^{o}$ to $\Delta=2.0^{o}$. Although this decreases the $\Delta\sigma$ values to more closely represent the experimentally observed average, it still fails to reproduce the experimental distribution of $\Delta\theta_{max}$ values.

Confidence Intervals for linear fits: Confidence intervals (95%) for each of the linear fits are shown below in Table 2. A linear fit is not expected to accurately represent the correlation between property changes and initial properties. The linear fit is only used to determine if a positive or negative correlation could be claimed between certain properties and their changes after treatment. If both the upper and lower bound of the confidence intervals are negative, then a negative correlation is claimed, and if both bounds are positive, then a positive correlation is claimed. Otherwise, if the lower bound is negative, and the upper bound is positive, no correlation is claimed.

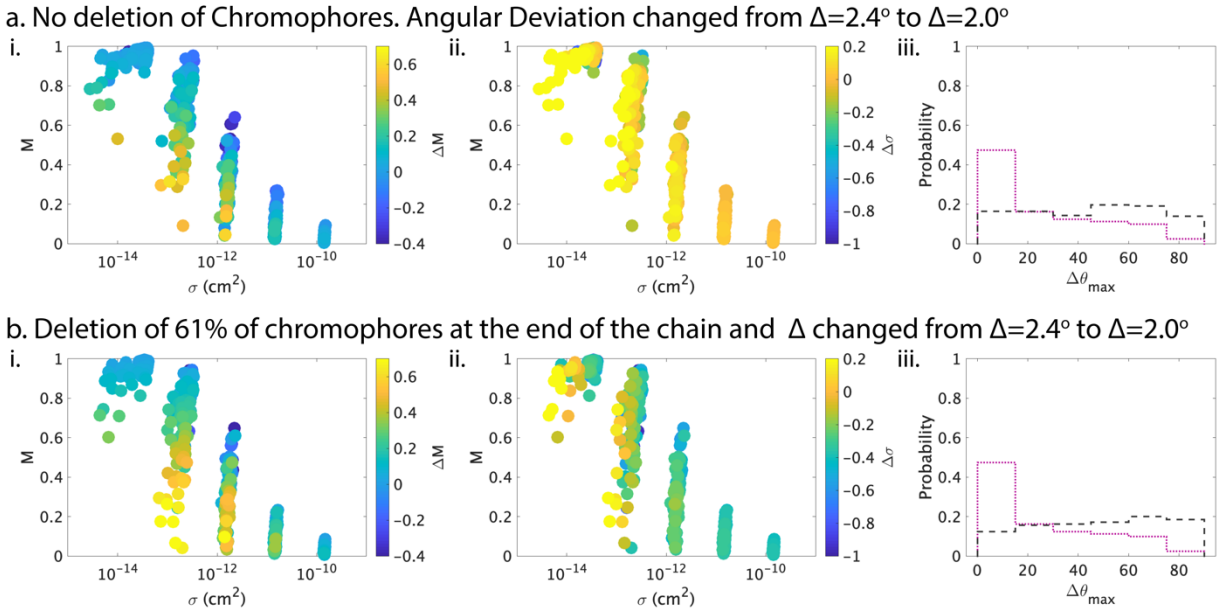

Figure S5. Color plots of the i) ΔM and ii) Δσ after varied chromophore deletions for each particle plotted against the simulated M and σ of each particle before chromophore deletion. Histograms (iii) of simulated peak angle changes (■) are compared to the experimentally observed values (■). a) No chromophores were deleted and Δ was changed from Δ=2.4° to Δ=2.0° to simulate increased crystallinity in the simulated chain. b) The last 61% of chromophores at the end of the chain were deleted and Δ was changed for the remaining chromophores from Δ=2.4° to Δ=2.0° to simulate increased crystallinity in the simulated chain.

Table S2. Linear fits and confidence intervals (95%) bounds of various properties and changed in properties after a treatment						
Figure	Treatment type	x axis	y axis	Slope	Lower bound (Confidence 95%)	Upper bound (Confidence 95%)
SI 7a	Thermal	ΔM	$\Delta\theta_{max}$	-23.732	-40.292	-7.172
SI 7a	Thermal	ΔM	$\Delta\theta_{max}$ if M>0.2	-14.872	-28.084	-1.660
SI 7b	DMSO	ΔM	$\Delta\theta_{max}$	24.669	-3.922	53.259
SI 7b	DMSO	ΔM	$\Delta\theta_{max}$ if M>0.2	24.392	-6.484	55.267
SI 7c	Thermal	$\Delta\sigma$	$\Delta\theta_{max}$	-2.181	-9.959	5.596
SI 7c	Thermal	$\Delta\sigma$	$\Delta\theta_{max}$ if M>0.2	-4.663	-11.103	1.777
SI 7d	DMSO	$\Delta\sigma$	$\Delta\theta_{max}$	-6.562	-22.865	9.741
SI 7d	DMSO	$\Delta\sigma$	$\Delta\theta_{max}$ if M>0.2	-6.523	-25.486	12.439
4a	Thermal	σ	$\Delta\sigma$	0.022	-0.039	0.082
4b	Thermal	σ	ΔM	-0.014	-0.042	0.013
SI 6a	Thermal	σ	$\Delta\theta_{max}$	0.354	-2.404	3.112
SI 6a	Thermal	σ	$\Delta\theta_{max}$ if M>0.2	-2.066	-4.314	0.182
5a	DMSO	σ	$\Delta\sigma$	-0.057	-0.166	0.052
5b	DMSO	σ	ΔM	-0.068	-0.128	-0.008
SI 6b	DMSO	σ	$\Delta\theta_{max}$	-15.264	-22.457	-8.071
SI 6b	DMSO	σ	$\Delta\theta_{max}$ if M>0.2	-2.066	-23.863	-7.916
4c	Thermal	M	$\Delta\sigma$	-0.003	-0.187	0.180
4d	Thermal	M	ΔM	-0.063	-0.146	0.021
SI 6c	Thermal	M	$\Delta\theta_{max}$	-14.824	-22.758	6.889
SI 6c	Thermal	M	$\Delta\theta_{max}$ if M>0.2	-6.582	-13.954	0.791
5c	DMSO	M	$\Delta\sigma$	-0.201	-0.535	0.132
5d	DMSO	M	ΔM	-0.359	-0.530	-0.187
SI 6d	DMSO	M	$\Delta\theta_{max}$	2.569	-21.885	27.022
SI 6d	DMSO	M	$\Delta\theta_{max}$ if M>0.2	-6.582	-13.199	48.393

Additional Correlations: In addition to comparing the ΔM and Δσ due to treatment against the initial M and σ before treatments (shown as Figures 4 and 5 in the main text), the $\Delta\theta_{max}$ were also compared to the initial M and σ pictured below. For the thermal anneal, no significant dependence was shown on either M or σ for the $\Delta\theta_{max}$ (Figure S6). For the DMSO anneal (Figure S7), no dependence on M was seen for $\Delta\theta_{max}$. However, $\Delta\theta_{max}$ does have a negative correlation with σ even with the exclusion of points with M<0.2 due to low signal to noise (shown as light

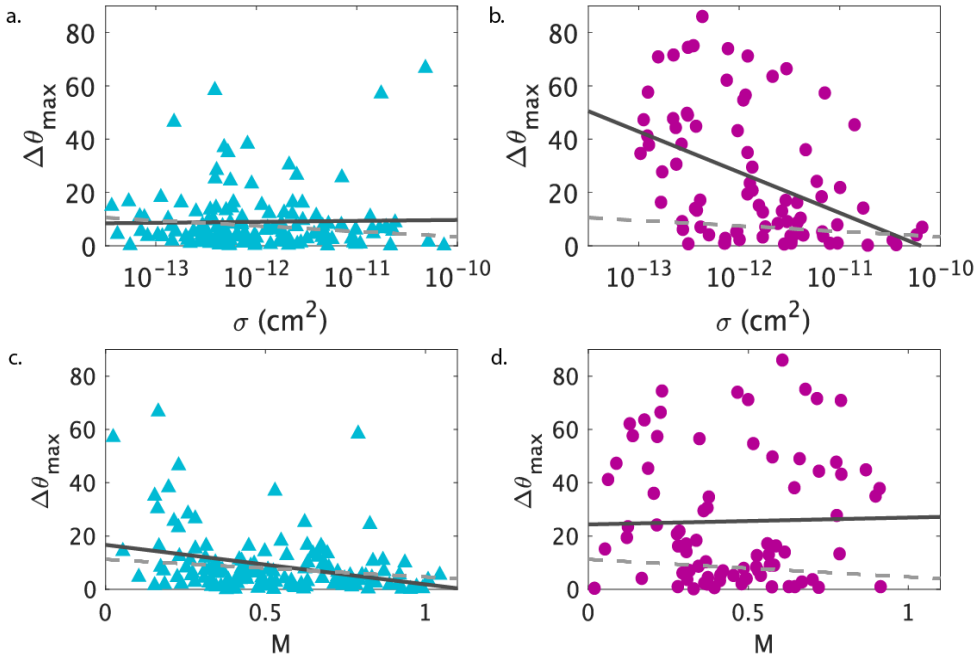

Figure S6. a) Comparison of $\Delta\theta_{max}$ after the thermal anneal to the σ of the pristine particle before annealing. b) Comparison of $\Delta\theta_{max}$ after the DMSO treatment to the σ of the particle after the thermal anneal. c) Comparison of $\Delta\theta_{max}$ after the thermal anneal to the M of the pristine particle. d) Comparison of $\Delta\theta_{max}$ after the DMSO treatment to the M of the particle after the thermal anneal. The dark grey lines are a linear fit of the data while the lighter dashed grey lines are a linear fit of the data excluding data points with M < 0.2 because a low M makes it difficult to determine the θ_{max} due to low signal to noise.

grey dashed lines).

Additionally, the $\Delta\theta_{max}$ was compared to the ΔM and $\Delta\sigma$ for each treatment, shown below. For the thermal anneal, a negative correlation was observed between $\Delta\theta_{max}$ and ΔM even with exclusion of points where $M<0.2$. No such correlation is observed comparing $\Delta\theta_{max}$ to $\Delta\sigma$, however. For the DMSO treatment, no significant correlations between the $\Delta\theta_{max}$ and either ΔM or $\Delta\sigma$ were observed.

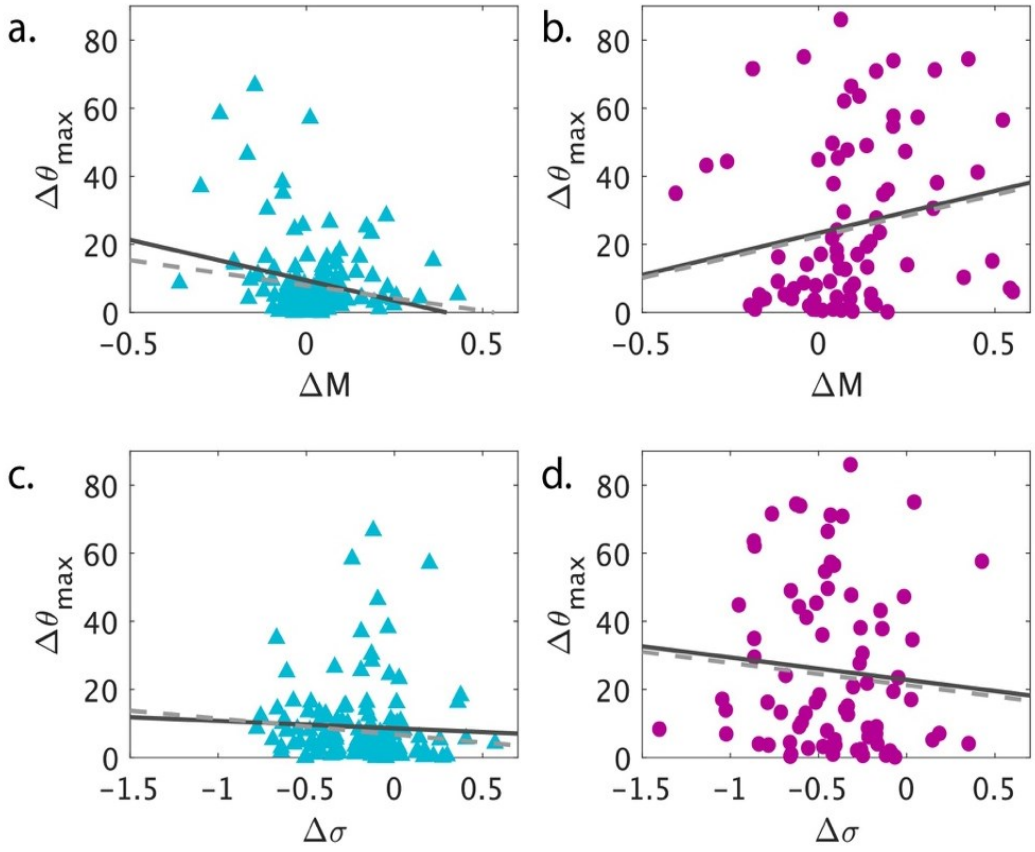

Figure S7. Peak angle changes ($\Delta\theta_{max}$) after thermal (■) and DMSO (■) treatments are compared to the (a,b) ΔM and (c,d) $\Delta\sigma$ after each treatment for each object. The dark grey lines are a linear fit of the data while the lighter dashed grey lines are a linear fit of the data excluding data points with $M < 0.2$ because a low M makes it difficult to determine the θ_{max} due to low signal to noise.

Multiple Variable Linear Regression for Figure 6: In addition to establishing a correlation between the ΔM or $\Delta\sigma$ against a single variable, a multiple linear regression was performed between ΔM or $\Delta\sigma$ and M and σ. A negative correlation was seen with ΔM against both M and σ

within the 95% confidence intervals, suggesting a negative correlation where ΔM tends to decrease with larger (greater σ), more ordered (greater M) objects, Figure 6a. For Δσ dependence on M and σ, since the slope crosses zero within the 95% confidence bounds, no positive or negative relationship can be claimed with certainty, Figure 6b.

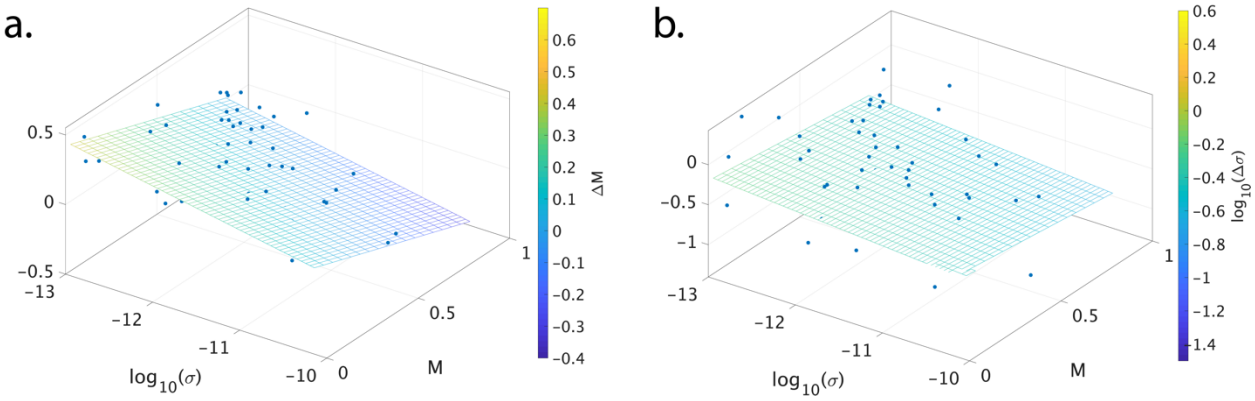

Figure S8. Experimental data (blue) of a) ΔM or b) Δσ values plotted against the M and σ before DMSO exposure. The data is fit using a multivariable regression, plotted as a color mesh.

Table S3. Linear fits and confidence intervals (95%) bounds of various properties and changed in properties after a treatment after multiple linear regression with independent variables M and σ						
Figure	Treatment type	x or y axis	z (color) axis	Slope	Lower bound (Confidence 95%)	Upper bound (Confidence 95%)
SI 8a	DMSO	σ	ΔM	-.1159	-.1688	-.0629
SI 8a	DMSO	M	ΔM	-.4695	-.6320	-.3070
SI 8b	DMSO	σ	Δσ	-.0858	-.1995	0.0278
SI 8b	DMSO	M	Δσ	-.2837	-.6323	0.0649

Absorption Coefficient Calculation from Resonance Shift: As mentioned in the Methods, COMSOL simulations are used to convert a resonance shift into an absorption cross section of the deposited PEDOT:PSS particles on different parts of the toroidal microresonator and have been described previously[1-2, 6-7]. Briefly, the thermal response of the toroid is simulated using the Heat Transfer Module of COMSOL where heat transfer from a point source on the microresonator is simulated to yield a temperature distribution of the toroid (and thus a refractive

index distribution). This simulation is repeated several times where the point source position is varied to account for particles depositing on different parts of the microresonator. In a separate simulation, the fundamental optical mode is simulated in COMSOL. The shift in resonance frequency is then calculated by overlapping the fundamental mode and temperature distribution of the toroid and scaling by the thermo-optic coefficient of silica to relate a change in temperatures to a shift in resonance frequency of the toroid. Thus, because the location of the object is known, dissipated heat can then be related to the resonance shift of the toroid. When the excitation intensity (by measuring the power and spot size) and quantum yield of thermalization (~100% for PEDOT:PSS) are also known, the absorption cross section of the object can be quantitatively determined. This process has been shown to produce cross sections that quantitatively agree with known absorption cross sections for carbon nanotubes and gold nanorods[1, 7].

Treatment Effects on Microresonators: To ensure that the property changes of the PEDOT:PSS from the thermal and DMSO exposures came from changes to the nanoparticles and not changes to the microresonator, behaviors of three different microresonators were monitored over several days both before treatment, after thermal anneal, and after DMSO exposure. This was performed by photoexciting the silicon pillar of the microresonator with a 633 nm laser and measuring the resonance shift produced by silicon's absorption of visible light. This procedure essentially quantifies the photothermal response of the resonator. The average resonance shift of each pillar and its standard deviation are in Table S4. Toroid A was measured 10 times throughout 19 days before treatment, 5 times over 6 days after the thermal anneal, and 3 times over 3 days after the DMSO exposure. Toroid B was measured 7 times throughout 19 days before treatment, 2 times over 7 days after the thermal anneal, and 2 times in one day after the DMSO exposure. The

subsequent average resonance shifts of the pillars are within one standard deviation of the pillar's average resonance shifts before treatment, suggesting that no significant changes in the toroid occur with treatment.

Table S4. Average Resonance Shift of resonator pillar and its standard deviation before treatment, after thermal annealing, and after DMSO exposure.

	Average Resonance Shift of resonator pillar (fm) before treatment	Standard Deviation of Resonance Shift of resonator pillar (fm) before treatment	Average Resonance Shift of resonator pillar (fm) after thermal anneal	Standard Deviation of Resonance Shift of resonator pillar (fm) after thermal anneal	Average Resonance Shift of resonator pillar (fm) after DMSO exposure	Standard Deviation of Resonance Shift of resonator pillar (fm) after DMSO exposure
Toroid A	2.578	0.464	2.945	0.261	2.873	0.266
Toroid B	2.597	0.640	3.058	0.476	2.947	0.064

Reproducibility of Data: To explore the reproducibility of our data, photothermal measurements were repeatedly taken on five different PEDOT:PSS objects before any thermal or DMSO annealing. Some uncertainty is to be expected due to taper drift (change in coupling between the taper and toroid as the taper drifts away from the toroid due to air currents) which is actively corrected for during experiments. Object A was measured 10 times throughout 19 days, except for the M and θ_{max} which were only measured 9 times. Object B was measured 6 times throughout 17 days, except for the M and θ_{max} which were only measured 3 times. Object C was measured 6 times throughout 17 days, except for the M and θ_{max} which were only measured 3 times. Object D was measured 7 times throughout 17 days, except for the M and θ_{max} which were only measured 3 times. Object E was measured 8 times throughout 17 days, except for the M and θ_{max} which were only measured 5 times. One sees that the average properties of M and θ_{max} remained consistent and with smaller standard deviations. This is also true for σ although Object E does have larger relative standard deviation compared to the other objects for unknown reasons. The average M and σ standard deviations are plotted in Figure S9.

PEDOT:PSS Object	Average σ (cm^2)	Standard Deviation of σ	Average M	Standard Deviation of M	Average θ_{max}	Standard Deviation of θ_{max}
A	1.08E-11	2.25E-12	0.32	0.01	32.24	1.38
B	4.32E-14	1.17E-14	0.84	0.03	160.18	2.02
C	2.151E-12	2.56E-13	0.77	0.01	98.82	1.70
D	2.28E-12	3.96E-13	0.43	0.01	176.20	2.73
E	1.48E-13	5.76E-14	0.43	0.17	146.24	6.58

Additional Figures:

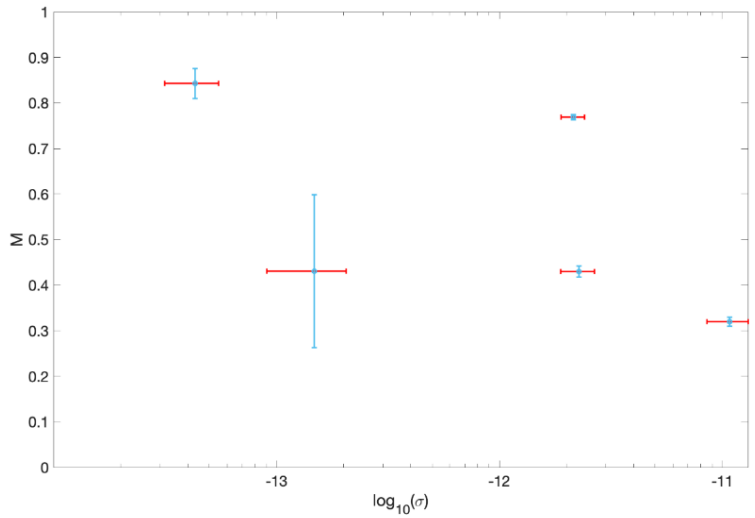

Figure S9. Average M and σ with standard deviations as error bars of objects A through E.

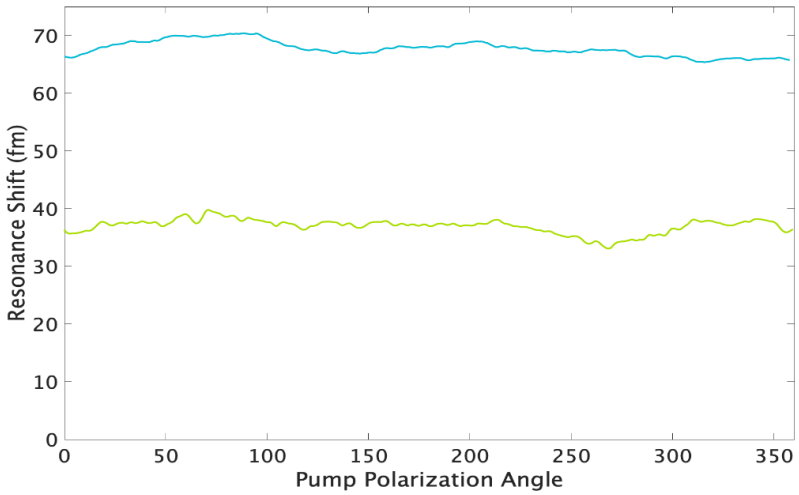

Figure S10. Polarization spectra of a low M object before treatment (■) and after the thermal (■) treatment. The low M makes it difficult to assign a θ_{max}.

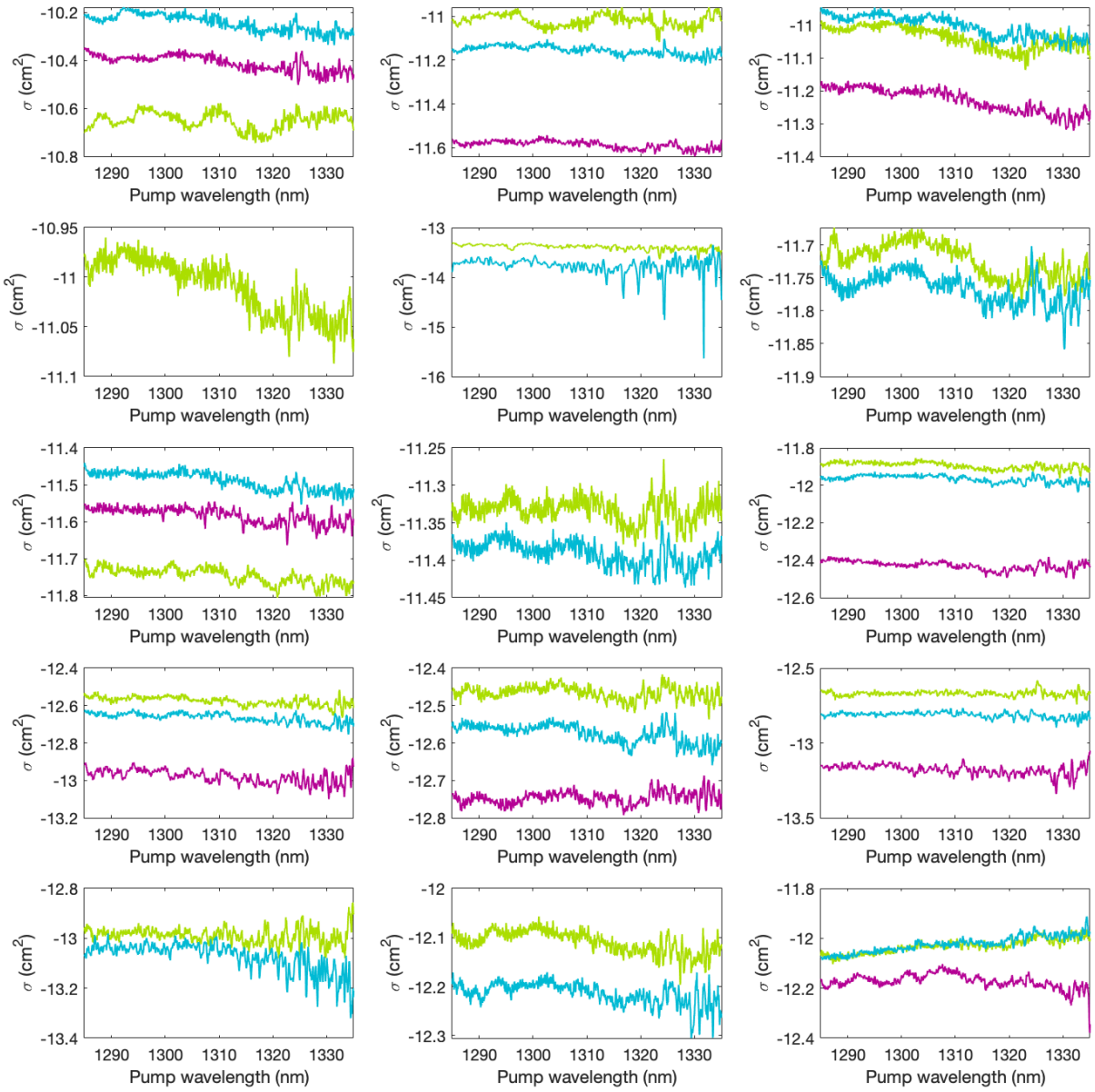

Figure S11. Representative absorption spectra of PEDOT:PSS before treatment (■) and after the thermal (■) and DMSO (■) treatments. The spectra remain relatively flat in the NIR range with no dramatic emergence or disappearance or spectral peaks observed within experimental noise, which is largely caused by the tapered optical fiber carrying the probe beam drifting from the toroid.

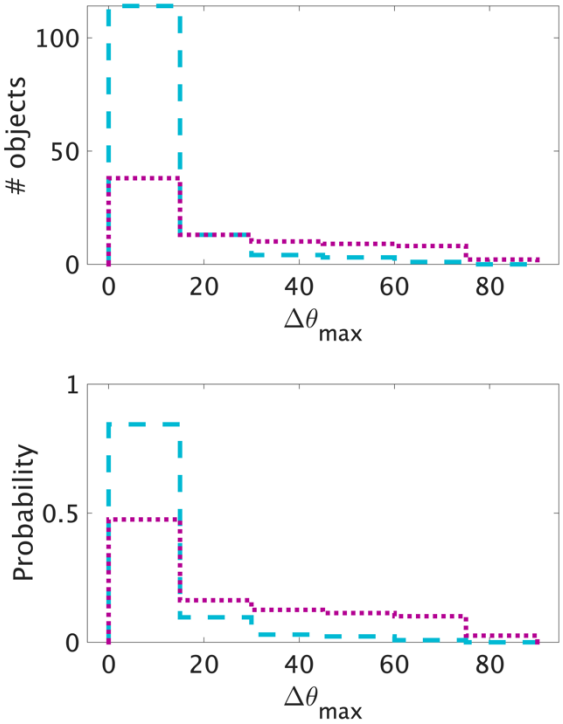

Figure S12. Histograms of $\Delta\theta_{max}$ after the thermal (■) and DMSO (■) treatments based on a) absolute number of objects and b) normalized by probability.

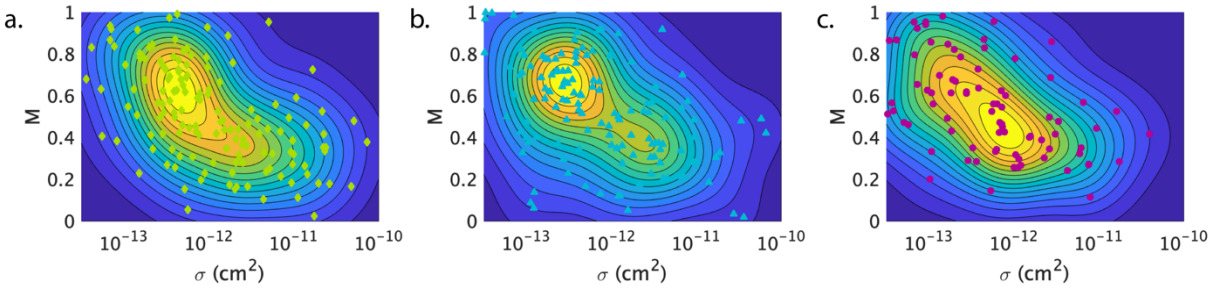

Figure S13. Density distributions of the experimentally observed depth of modulations (M) and absorption cross sections (σ) for all objects, including those that do not survive subsequent treatment. Individual objects are represented by the blue-green-yellow contour plot, with experimentally observed values plotted as points for the a) pristine (◆), b) thermally annealed (▲), and c) DMSO-treated objects for all objects (●).

References:

1. Heylman, K. D.; Thakkar, N.; Horak, E. H.; Quillin, S. C.; Cherqui, C.; Knapper, K. A.; Masiello, D. J.; Goldsmith, R. H., Optical microresonators as single-particle absorption spectrometers. *Nat. Photonics* **2016,** *10*, 788.
2. Horak, E. H.; Rea, M. T.; Heylman, K. D.; Gelbwaser-Klimovsky, D.; Saikin, S. K.; Thompson, B. J.; Kohler, D. D.; Knapper, K. A.; Wei, W.; Pan, F.; Gopalan, P.; Wright, J. C.; Aspuru-Guzik, A.; Goldsmith, R. H., Exploring Electronic Structure and Order in Polymers via Single-Particle Microresonator Spectroscopy. *Nano Lett.* **2018,** *18*, 1600-1607.
3. Bolinger, J. C.; Traub, M. C.; Brazard, J.; Adachi, T.; Barbara, P. F.; Vanden Bout, D. A., Conformation and Energy Transfer in Single Conjugated Polymers. *Acc. Chem. Res.* **2012,** *45*, 1992-2001.
4. Hunter, G. L.; Edmond, K. V.; Elsesser, M. T.; Weeks, E. R., Tracking rotational diffusion of colloidal clusters. *Opt. Express* **2011,** *19*, 17189-17202.
5. Wang, C.; Duong, D. T.; Vandewal, K.; Rivnay, J.; Salleo, A., Optical measurement of doping efficiency in poly (3-hexylthiophene) solutions and thin films. **2015,** *085205*, 1-7.
6. Thakkar, N.; Rea, M. T.; Smith, K. C.; Heylman, K. D.; Quillin, S. C.; Knapper, K. A.; Horak, E. H.; Masiello, D. J.; Goldsmith, R. H., Sculpting Fano Resonances To Control Photonic–Plasmonic Hybridization. *Nano Lett.* **2017,** *17*, 6927-6934.
7. Heylman, K. D.; Knapper, K. A.; Goldsmith, R. H., Photothermal microscopy of nonluminescent single particles enabled by optical microresonators. *J. Phys. Chem. Lett.* **2014,** *5*, 1917-1923.